Examining the nuclear mass surface of Rb and Sr isotopes in the $A \approx 104$ region via precision mass measurements

I. Mukul,[1,*] C. Andreoiu,[2] J. Bergmann,[3] M. Brodeur,[4] T. Brunner,[1,5] K. A. Dietrich,[1,6] T. Dickel,[3,7] I. Dillmann,[1,8] E. Dunling,[1,9] D. Fusco,[1,10] G. Gwinner,[11] C. Izzo,[1] A. Jacobs,[1,12] B. Kootte,[1,11] Y. Lan,[1,12] E. Leistenschneider,[1,12] E. M. Lykiardopoulou,[1,12] S. F. Paul,[1,6] M. P. Reiter,[1,3,13] J. L. Tracy, Jr.,[1] J. Dilling,[1,12] and A. A. Kwiatkowski[1,8]

[1]*TRIUMF, 4004 Wesbrook Mall, Vancouver, British Columbia V6T 2A3, Canada*
[2]*Department of Chemistry, Simon Fraser University, Burnaby, British Columbia V5A 1S6, Canada*
[3]*II. Physikalisches Institut, Justus-Liebig-Universität, Gießen 35392, Germany*
[4]*Department of Physics, University of Notre Dame, Notre Dame, Indiana 46556, USA*
[5]*Department of Physics, McGill University, Montréal, Québec H3A 2T8, Canada*
[6]*Ruprecht-Karls-Universität Heidelberg, Heidelberg D-69117, Germany*
[7]*GSI Helmholtzzentrum für Schwerionenforschung GmbH, Darmstadt D-64291, Germany*
[8]*Department of Physics and Astronomy, University of Victoria, Victoria, British Columbia V8P 5C2, Canada*
[9]*Department of Physics, University of York, York YO10 5DD, United Kingdom*
[10]*Department of Physics, University of Waterloo, Ontario N2L 3G1, Canada*
[11]*Department of Physics and Astronomy, University of Manitoba, Winnipeg, Manitoba R3T 2N2, Canada*
[12]*Department of Physics and Astronomy, University of British Columbia, Vancouver, British Columbia V6T 1Z1, Canada*
[13]*School of Physics and Astronomy, University of Edinburgh, Edinburgh EH9 3FD, United Kingdom*

(Received 3 January 2021; accepted 15 April 2021; published 28 April 2021)

Background: The neutron-rich $A \approx 100$, $N \approx 62$ mass region is important for both nuclear structure and nuclear astrophysics. The neutron-rich segment of this region has been widely studied to investigate shape coexistence and sudden nuclear deformation. However, the absence of experimental data of more neutron-rich nuclei poses a challenge to further structure studies. The derivatives of the mass surface, namely, the two-neutron separation energy and neutron pairing gap, are sensitive to nuclear deformation and shed light on the stability against deformation in this region. This region also lies along the astrophysical *r*-process path, and hence precise mass values provide experimental input for improving the accuracy of the *r*-process models and the elemental abundances.

Purpose: (a) Changes in deformation are searched for via the mass surface in the $A = 104$ mass region at the $N = 66$ mid-shell crossover. (b) The sensitivity of the astrophysical *r*-process abundances to the mass of Rb and Sr isotopic chains is studied.

Methods: Masses of radioactive Rb and Sr isotopes are precisely measured using a Multiple-Reflection Time-of-Flight Mass Separator (MR-TOF-MS) at the TITAN facility. These mass values are used to calculate two-neutron separation energies, two-neutron shell gaps and neutron pairing gaps for nuclear structure physics, and one-neutron separation energies for fractional abundances and astrophysical findings.

Results: We report the first mass measurements of ^{103}Rb and $^{103-105}$Sr with uncertainties of less than 45 keV/c^2. The uncertainties in the mass excess value for ^{102}Rb and ^{102}Sr have been reduced by a factor of 2 relative to a previous measurement. The deviations from the AME extrapolated mass values by more the 0.5 MeV have been found.

Conclusions: The metrics obtained from the derivatives of the mass surface demonstrate no existence of a subshell gap or onset of deformation in the $N = 66$ region in Rb and Sr isotopes. The neutron pairing gaps studied in this work are lower than the predictions by several mass models. The abundances calculated using the waiting-point approximation for the *r* process are affected by these new masses in comparison with AME2016 mass values.

DOI: 10.1103/PhysRevC.103.044320

I. INTRODUCTION

Nuclei far from stability are important for both nuclear astrophysics and nuclear structure physics. The synthesis of nearly half of the elements heavier than iron has been attributed to the rapid neutron-capture process [1–5], named the *r* process, for which an enormous flux of neutrons is required. The site for the *r* process has been a matter of discussion in the past [1,4], as this site can be validated from a source of freshly synthesized elements, e.g. a neutron-star merger. Incidentally, the multimessenger astronomy of the recent

*ishmukul@gmail.com

binary star merger GW170817 [6–8] showed the conditions for the *r* process, and the kilonova AT2017gfo recorded in the following days provided the evidence of synthesis of the *r*-process elements, which validated neutron-star mergers as one of the possible *r*-process sites. One of the detailed analyses from AT2017gfo also identified strontium in the merger of two neutron stars [9] and established its importance in *r*-process calculations.

The formation of neutron-rich atoms is a competition of neutron capture, β decay, and photodisintegration [10]. Starting from a seed nucleus, neutron capture dominates up to a so-called waiting point whose neutron separation energy is low enough to allow β decay to become dominant. The site for these waiting points in the nuclear chart is not known exactly. However, precise experimental values for all the physical phenomena involved are required to pin down these sites. Abundances obtained by large-scale *r*-process network calculations are directly affected by the precision in measurement of the ground-state properties of a nucleus, including atomic mass, β-decay properties, neutron capture rates, β-delayed neutron emission, and fission distributions [11]. Of these variables, the atomic mass is considered to be highly sensitive for the *r*-process path calculations [12]. Due to the exotic nature of the *r*-process nuclei, their masses are generally unknown (unmeasured or with large uncertainties), and most calculations rely on the mass models. The commonly used models in *r*-process calculations, e.g., Duflo-Zuker [13], the finite range droplet model (FRDM12) [14], and Hartree-Fock-Bogoliubov (HFB-24) [15], are generally optimized on the experimentally available data with a root-mean-square error of less than 1 MeV. The mass data groups, for example, the atomic mass evaluation (AME2016) [16], also publish extrapolated values for exotic nuclei based on their large database. However, it is important to constrain mass models by providing more experimental values with good accuracy.

On the nuclear structure side, neutron-rich isotopes in the $A = 100$ region are known for changes in nuclear shapes evident by measurements involving charge radii [17–21], by nuclear moments extracted from isotope shifts and hyperfine structure studies by laser spectroscopy [18,19,21–23], and by theory [24,25]. This region is also explored with measurements of mass [26–31] and its derivative, two-neutron separation energy S_{2n}, which is sensitive to nuclear structure changes [32]. In an isotopic chain of a constant proton number, S_{2n} decreases smoothly with an increase in neutron number and drops sharply at the crossing of a closed neutron shell, indicating a magic neutron number. In the case of a shape transition, the slope of S_{2n} becoming positive gives a clear sign of shape transition or change in structure.

In the neutron-rich $A = 100$ region, a large change in trend is found in the S_{2n} values near $N = 62$ between isotopic chains of krypton ($Z = 36$) [27] and molybdenum ($Z = 42$) [29], creating a boundary of a deformed region. This deformed region also provides an opportunity to test the functionality of various nuclear models against nuclear deformation. The extrapolations from AME2016 evaluation for rubidium ($Z = 37$) and strontium ($Z = 38$) isotopes suggest another structure change based on the S_{2n} surface near the $N = 66$ mid-shell. This gives a strong impetus to explore nuclei crossing $N = 66$ and search for other shape transitions in this region.

The ideal and well-established tools for high-precision mass measurement of radioactive isotopes are ion traps [33,34]. We used TRIUMF's Ion Trap for Atomic and Nuclear science (TITAN) [35,36] for our measurements, which is a combination of different kinds of ion traps that are optimized for fast and precise mass measurements of short-lived nuclei. With the Multiple-Reflection Time-of-Flight Mass Separator (MR-TOF-MS) [37,38], TITAN is able to suppress isobaric contaminants and simultaneously perform high-precision mass measurements. In this article, we report the mass measurements of $^{99–103}$Rb and $^{99–105}$Sr using the MR-TOF-MS, where ^{103}Rb and $^{103–105}$Sr were measured for the first time. The effects of the derivatives of the deduced mass surface on nuclear structure and astrophysical *r*-process abundance calculations are reported here.

II. EXPERIMENTAL DETAILS

The experiment was performed using the recently commissioned MR-TOF-MS [37,38] at the TITAN facility at TRIUMF. The rare isotope beams of rubidium and strontium were produced at the Isotope Separator and Accelerator (ISAC) [39] facility at TRIUMF by impinging 480 MeV protons of 9.8 μA intensity onto a uranium carbide target [40]. The produced atomic species were ionized by a surface ion source and, for Sr, TRIUMF's Resonant Laser Ionization Ion Source (TRILIS) [41]. The singly charged ions were then accelerated to an energy of 20 keV and passed through a dipole magnet for mass selection. The mass resolving power ($m/\delta m$) at this stage is up to 3000 [39], which is sufficient for separating isotopes at a single mass unit. The filtered beam of interest was directed toward the experimental area of TITAN and injected into its radio-frequency quadrupole cooler and buncher (TITAN RFQ) [42,43]. The radioactive ion beam (RIB) was accumulated inside the TITAN RFQ for 20 ms, extracted in cooled bunches, and sent toward the MR-TOF-MS for mass measurement.

The initial sections of the MR-TOF-MS consist of an injection trap [44], where ions were recooled by collision with helium gas, for injection into the electrostatic time-of-flight mass analyzer [45]. In the MR-TOF-MS, the flight path and in turn time of flight for the ion bunches was increased by trapping the ion bunch between two electrostatic isochronous mirrors. The electric potentials on mirrors were chosen such that the initial time spread was preserved during this long travel path [46]. In this way, a long time of flight was achieved inside a compact device.

In the present experiment, the MR-TOF-MS was operated in duty cycles of 20 ms. The ions were cooled in the injection trap for nearly 13 ms, and, in turn, were injected into the mass analyzer section where they underwent 396 isochronous turns before being detected by a MagneTOF detector. A time-focus-shift (TFS) turn [47] was used to focus the TOF onto the MagneTOF detector. The FWHM of peaks produced by different isotopes in TOF spectra were nearly 20 ns FWHM after a flight time of nearly 7.8 ms. The mass resolving power achieved in this experiment was $\approx$185 000. The typical

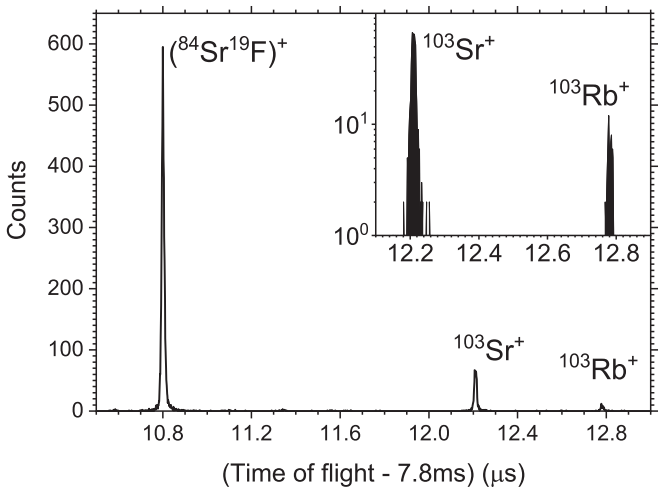

FIG. 1. A time-of-flight spectrum of $^{103}Rb^+$ and $^{103}Sr^+$ ions after 386 turns inside TITAN's MR-TOF-MS. Inset: Zoomed area containing $^{103}Sr^+$ and $^{103}Rb^+$ ions on a logarithmic scale. $^{84}Sr\,^{19}F^+$ served as calibration species for conversion from time to mass. The spectrum contains data from a single file. Multiple files were recorded and analyzed for final masses.

peak shape in the MR-TOF-MS spectra, shown in Fig. 1, is well described by a Gaussian distribution. The time-of-flight spectra were calibrated to mass spectra using the calibration function,

$$m/q = c\,(t - t_0)^2 \tag{1}$$

with c and t_0 being the calibration parameters, and m, q, and t being the mass, charge, and time of flight of the ion of interest (IOI), respectively. The time offset t_0 depended on delays due to signal processing and electronics used and hence is constant for the experiment. $t_0 = 167(2)$ ns was determined before the start of the RIB experiment using $^{85}Rb^+$, $^{87}Rb^+$, and $^{133}Cs^+$ ions undergoing a single TFS turn. The parameter c is a device-specific parameter that depends on the energy of the ions and the total path length. c was calculated using a precisely measured isobaric reference ion present in each RIB measurement that underwent the same number of turns as the ion of interest. These reference ions are generally a stable atomic or molecular species in the same spectra and are tabulated in Table I.

Another technique used in this experiment was mass-selective retrapping [48], since the intensity of the IOI was 10^2 times less than the contamination. After a few turns inside the mass analyzer section, the IOI was dynamically recaptured inside the injection trap, with the capture time chosen to optimize capture of the IOI while rejecting unwanted species. Ions in the injection trap were then recooled and released again into the mass analyzer. This technique suppressed ion-ion interactions, reducing systematic errors, and increased the dynamic range of the mass spectrometer. This technique was first used in an experiment to study neutron deficient ytterbium isotopes [49]. This method was successfully applied at mass numbers 104 and 105.

The uncertainties in measured masses were calculated as in [50]. The errors considered in our case were (a) the standard error of the centroid of Gaussian fitted peaks for calibrant and IOI, (b) a statistical error of $\sigma/\sqrt{N}$ for Gaussian fitted peaks of the calibrant, where σ is the width of Gaussian distribution and N is the number of counts in the peak, (c) the literature uncertainty of the calibration peak reported in AME2016 [16], and (d) the systematic uncertainty of the measurement device, $\delta m/m_{\rm sys} = 3 \times 10^{-7}$ [51]. This value is an upper limit derived from measurements using stable ions of $^{39,41}K^+$, before and after the experiment. The limit of systematic error is governed by the electric ringing of the voltages caused by the instabilities of the power supply used to eject ions from the mass analyzer section to the MagneTOF detector. All the aforementioned errors were added in quadrature to obtain the total error for each fitted spectrum. The effect of ion-ion interaction was negligible since the average ion count rate was less than one detected ion per cycle.

TABLE I. Half-lives [52] and mass excesses of $^{99-103}$Rb and $^{99-105}$Sr isotopes measured using TITAN's MR-TOF-MS, and the corresponding mass excess values ME_{TITAN} and values from AME2016 [53] ($ME_{AME2016}$), as well as their difference $\Delta_{TITAN\text{-}AME2016}$. The last column shows the results from a recent ISOLTRAP measurement [30]. The label # in the AME2016 values indicates an extrapolated value. All ions were singly charged. All mass excess values have been rounded to the nearest integer.

Isotope	Half-life (ms)	Calibration ion	ME_{TITAN} (keV/c^2)	$ME_{AME2016}$ (keV/c^2)	$\Delta_{TITAN\text{-}AME2016}$ (keV/c^2)	$ME_{ISOLTRAP}$ (keV/c^2)
^{99}Rb	54(4)	^{99}Mo	−51101(31)	−51121(4)	20(31)	
^{100}Rb	51(8)	^{100}Ru	−46243(30)	−46247(20)	4(35)	−46290(19)
^{101}Rb	32(5)	^{101}Ru	−42480(29)	−42845#(200#)	365(202)	−42558(28)
^{102}Rb	37(5)	^{102}Ru	−37241(29)	−37707#(300#)	466(301)	−37253(83)
^{103}Rb	23(13)	^{84}Sr ^{19}F	−33049(32)	−33608#(401#)	559(402)	
^{99}Sr	269(1)	^{99}Mo	−62509(31)	−62521(5)	13(31)	
^{100}Sr	202(3)	^{100}Ru	−59824(29)	−59821(7)	−3(30)	−59827(27)
^{101}Sr	118(3)	^{101}Ru	−55311(29)	−55325(8)	14(30)	−55315(21)
^{102}Sr	69(6)	^{102}Ru	−52175(29)	−52160(70)	−15(76)	−52160(67)
^{103}Sr	53(10)	^{84}Sr ^{19}F	−47220(29)	−47420#(198#)	200(200)	
^{104}Sr	53(5)	^{104}In	−43411(33)	−44110#(300#)	699(302)	
^{105}Sr	39(5)	^{105}Pd	−37886(44)	−38610#(503#)	724(505)	

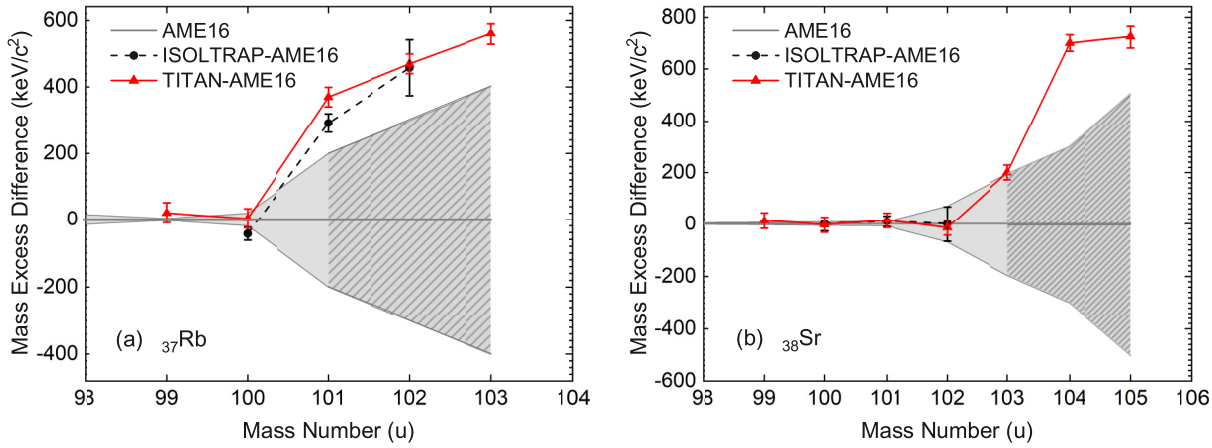

FIG. 2. Mass excess difference between the value measured in this work and the value reported in AME2016 [16], i.e., $ME_{TITAN} - ME_{AME2016}$ for (a) $_{37}$Rb and (b) $_{38}$Sr isotopes. The shaded band indicates the AME2016 uncertainties, and slanted lines in the shaded region denote values from extrapolation. ME difference is also plotted for a previous measurement from ISOLTRAP [30], published after the AME2016.

The final mass values from this work are tabulated in Table I, and are compared with literature values of AME2016 [16] and, where possible, previous measurements from ISOLTRAP's Penning trap and MR-TOF-MS [30].

III. RESULTS: MASS VALUES

The atomic masses of $^{99-103}$Rb and $^{99-105}$Sr were measured with the MR-TOF-MS. A few masses reported herein have been previously measured with Penning trap facilities at TITAN and other laboratories. For each mass unit, we used a calibrant that has been measured very precisely, with a few keV or less. In the case of unavailability of an atomic calibrant, a precisely known molecular species was used.

The mass values in atomic mass units, obtained from the data analysis, were converted into the mass excess (ME) values defined as the difference between the calculated mass M and atomic mass number $A = N + Z$, i.e., $ME(N, Z) = [M(N, Z) - A(N, Z)]$, expressed in units of keV/c^2. The ME values from this work are tabulated in Table I and plotted in Fig. 2, against the existing literature values [16]. The following subsections provide a detailed comparison of direct mass measurements for Rb and Sr isotopes with previous results if existing.

A. ^{99}Rb and ^{99}Sr

^{99}Rb has been measured using the Penning Trap Mass Spectrometer (PTMS) at TITAN [31] and ISOLTRAP [29], resulting in an AME2016 value of $-51121(4)$ keV/c^2. The ME value in this measurement was found to be $-51101(31)$ keV/c^2, which agrees within 20 keV/c^2 (0.7σ) of AME2016. At this mass unit, atomic ^{99}Mo$^+$ ($T_{1/2} = 65.9$ h, uncertainty $= 23$ keV/c^2) was used for calibration of the MR-TOF-MS spectrum.

^{99}Sr has been measured extensively using PTMS, measured twice at TITAN [28,31] and once at JYFLTRAP [26]. The mass value considering all measurements has been incorporated in AME2016 as $-62521(5)$ keV/c^2. The MR-TOF-MS mass value for ^{99}Sr is $-62509(31)$ keV/c^2, within 12 keV (0.4σ) of the AME2016 value.

B. ^{100}Rb and ^{100}Sr

The atomic mass of ^{100}Rb was previously measured using PTMS [29] and MR-TOF-MS [30] at ISOLTRAP with values of $-46247(20)$ and $-46290(19)$ keV/c^2, respectively. The value using PTMS at TITAN [31] was $-46190(140)$ keV/c^2, where the large uncertainty was attributed to the high contamination. Our new mass excess value from MR-TOF-MS was found to be $-46243(30)$ keV/c^2 which is in good agreement with AME2016 value of $-46247(20)$ keV/c^2 (0.1σ).

^{100}Sr has been measured using PTMS by ISOLTRAP [30] and TITAN [31]. The TITAN MR-TOF-MS value for ^{100}Sr is $-59824(29)$ keV/c^2, in agreement with the AME2016 value of $-59821(7)$ keV/c^2 (0.1σ). The calibration ion for $A = 100$ was stable ^{100}Ru$^+$ with an uncertainty of 0.3 keV/c^2).

C. ^{101}Rb and ^{101}Sr

^{101}Rb was previously measured using MR-TOF-MS at ISOLTRAP [30] with a value of $-42558(28)$ keV/c^2. The AME2016 for ^{101}Rb is an extrapolated value of $-42845(200\#)$. Our value of $-42480(29)$ keV/c^2 deviates by 78 keV/c^2 from ISOLTRAP and 365(202) keV/c^2 (1.8σ) from the AME2016 value.

^{101}Sr was previously measured using PTMS at TITAN [31] and ISOLTRAP [30], resulting in an AME2016 value of $-55325(8)$ keV/c^2. The mass excess measured by the TITAN MR-TOF-MS in this work is $-55311(29)$ keV/c^2, which is in agreement with previous works within 0.5σ deviation. The calibration ion for $A = 101$ was stable ^{101}Ru$^+$ with uncertainty $= 0.4$ keV/c^2.

D. ^{102}Rb and ^{102}Sr

Our new ME of ^{102}Rb was found to be $-37241(29)$ keV/c^2, which is in close agreement with the ISOLTRAP value of $-37253(83)$ keV/c^2. Both differ from the AME2016 value of $-37707(300\#)$ keV/c^2. The difference between TITAN and AME2016 values is 466(301) keV/c^2 which is a 1.6σ deviation.

^{102}Sr was previously measured at ISOLTRAP using PTMS, and that ^{102}Sr mass was used as calibrant to determine ^{102}Rb using MR-TOF-MS [30].

The ME value from ISOLTRAP PTMS for ^{102}Sr is $-52160(67)$ keV/c^2. We report a value of $-52175(29)$ keV/c^2, which is in agreement of 0.2σ with ISOLTRAP. The AME2016 used the ISOLTRAP value and thus agrees well with this work. The uncertainty in our work is reduced from the previous measurement of 67 keV/c^2 to 29 keV/c^2. The calibration ion at $A = 102$ was stable ^{102}Ru$^+$ with an uncertainty of 0.4 keV/c^2.

E. ^{103}Rb and ^{103}Sr

We report the first mass measurement of ^{103}Rb and ^{103}Sr. The values from AME2016 for ^{103}Rb, Sr are extrapolated values. The mass excess of ^{103}Rb was found to be $-33049(32)$ keV/c^2, which deviates from the AME2016 value of $-33608(401\#)$ keV/c^2 by 559(402) keV/c^2 (1.4σ). The mass excess for ^{103}Sr was found to be $-47220(29)$ keV/c^2, which agrees with AME2016 extrapolation value of $-47420(198\#)$ keV/c^2 within error bars (1σ). There was no atomic calibration ion present at this mass, and therefore the stable molecule ^{84}Sr ^{19}F$^+$ F$^+$ was used for calibration (uncertainty for ^{84}Sr = 1.2 keV/c^2 and for ^{19}F = 0.9 eV/c^2).

F. ^{104}Sr

We report the first mass measurement of ^{104}Sr. The AME2016 extrapolation is $-44110(300\#)$ keV/c^2. MR-TOF-MS was operated in mass-selective retrapping mode for this measurement. The mass excess value for ^{104}Sr is $-43411(33)$ keV/c^2. The deviation from the AME2016 value is 698(302) keV/c^2 (2.3σ).

The calibration ion used for this mass was ^{104}In$^+$ ($T_{1/2}$ = 1.8 min, uncertainty = 6 keV/c^2), with a known isomer of 93.48 keV/c^2 and $T_{1/2} = 15.7$ s [54]. We have followed AME2016's guidelines [16] for handling single isomer in calibration by adding half of the isomer's energy to mass value.

G. ^{105}Sr

We report the first direct mass measurement of ^{105}Sr. The AME2016 value of $-38610(503\#)$ keV/c^2 is an extrapolated value. MR-TOF-MS was operated in mass-selective retrapping mode for this measurement. The mass excess for ^{105}Sr was found to be $-37886(44)$ keV/c^2. The deviation from AME2016's extrapolation is 724(505) keV/c^2 (1.4σ). The calibration ion used at this mass was stable ^{105}Pd$^+$ with an uncertainty of 1.1 keV/c^2. A cross-check with ^{105}Ru$^+$ ($T_{1/2}$ = 4.4 hrs, uncertainty of 2.5 keV/c^2) as calibrant agreed within 4 keV/c^2.

IV. IMPACT ON THE MASS SURFACE AND ITS DERIVATIVES

The nuclear mass surface is derived by plotting atomic masses as a function of the proton (Z) and neutron (N) numbers. The surface is generally smooth and continuous if we neglect pairing effects. However, sudden changes in the surface may be caused by shell closures or change in shape or deformation of the ground state [32]. In order to reveal such changes in nuclear structure, it is important to study different derivatives of the mass surface, e.g., one- and two-neutron separation energies (S_n and S_{2n}), two-neutron shell gap energies (Δ_{2n}), and neutron-pairing gap energies (D_n). Out of these, S_n is a direct input in astrophysical calculations. In the following subsections, we will discuss these derivatives with our experimentally observed values and compare them with existing data and common mass models used for unknown masses in nuclear structure and astrophysical calculations.

A. Nuclear structure discussion

An important metric for probing nuclear structure is the two-neutron separation energy S_{2n} [32], which is calculated as $S_{2n} = -M(A, Z) + M(A-2, Z) + M(2n)$. S_{2n} removes the effect of odd-even staggering and gives a smoother trend. It generally decreases smoothly and continuously with increasing neutron number for an isotopic chain. A kink occurs at the shell closures. Abrupt changes in slope may occur at a shape change or onset of deformation in the ground state of the nuclide.

The region around $A = 100$ and $N = 60$ has been known for sudden shape transitions [55,56]. A shape change from spherical to oblate to prolate was deduced from experimental data on the charge radius [17] as well as by calculating the potential energy surfaces [24,25].

The behavior for Rb and Sr isotopes, along with neighboring Kr and Y, is shown in Fig. 3(a). This figure illustrates that in the isotopic chain of elements with $Z = 36$–39 there is a kink in the slope at $N = 50$ (shell closure), an abrupt increase in S_{2n} values with a local maximum at $N \approx 60$ (onset of deformation and shape change), and a smooth decrease thereafter. Isotopes with $N \geqslant 62$ were not well measured in this region; thus, the AME2016 values in this area have large uncertainties and in some cases are extrapolated. Our Rb and Sr measurements deviate from AME2016, evaluated and tabulated, leading to different S_{2n} values. From the $N = 50$ shell, the S_{2n} values of Rb and Sr isotopes follow a smooth slope till $N = 66$ for Rb isotopes and $N = 67$ for Sr isotopes, in agreement with a previous measurement at ISOLTRAP [30] up to $N = 65$ for Rb isotopes and $N = 64$ for Sr isotopes. The extrapolated values from AME2016 suggest a small kink near $N = 64$ indicating another change in nuclear structure; however, the smooth trend in our measured values refutes this expectation.

In order to flesh out minute structural information from the S_{2n} curves, we plot their slopes to reveal features, such as clear indicators of shell gaps or deformations. The two-neutron shell gap energy is given by $\Delta_{2n}(Z, N) = S_{2n}(Z, N) - S_{2n}(Z, N-2)$, which rises sharply and forms peak-like

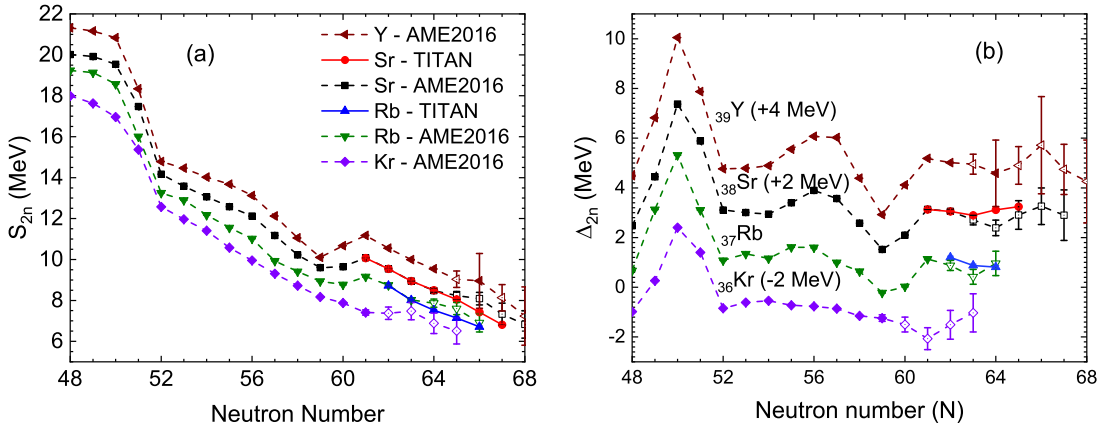

FIG. 3. (a) Two-neutron separation energy S_{2n} and (b) two-neutron shell gap Δ_{2n} as a function of neutron number for isotopic chains in the neighborhood of Rb and Sr. Δ_{2n} have been offset for clarity. The values measured in this work are shown by blue triangles (Rb) and red circles (Sr) connected by solid lines. AME2016 values are shown with different symbols and connected by the dashed line. Open symbols denote AME2016 extrapolations. Shell closure at $N = 50$ (peak) and shape transition at $N = 59$ (dip) are visible in both plots.

structures at shell closures. The Δ_{2n} can be negative, showing sudden changes in slope and the regions of deformation in the mass surface.

The Δ_{2n} values for Rb and Sr isotopes from this work, compared to AME2016 values, are shown in Fig. 3(b). The shell closure at $N = 50$ is clearly visible as a large peak, followed by a dip at $N = 59$ depicting the shape transition. AME2016 values predict another smaller dip near $N = 64$; however, the new TITAN measurements for Rb and Sr isotopes give nearly a smooth flat slope in the $N = 63$–67 region that signifies the stability of the nuclear shape in the measured isotopes.

Previously, the theoretical mass models estimated the mass surface in the experimentally unknown region to further many astrophysical studies [13–15]. Therefore, it is important to compare the validity of these models with the new experimental data. We compared our measured S_{2n} values with the values from commonly used mass models in r-process calculations, namely, Duflo-Zuker [13], FRDM2012 [14], and HFB24 [15]. In addition, we took values from four additional models, which belong to the class of self-consistent mean-field approaches [57] with two different effective interactions, namely Skyrme and Gogny. We took two parametrizations of the Skyrme interaction: UNEDF0 [58] and UNEDF1 [59]. The former includes adjustments for spherical and deformed nuclei, and the latter is optimized for excitation energy of fission isomers. For other interaction (Gogny), only D1S parametrization is used [60,61]. For Sr isotopes (being even Z), a beyond mean-field approach is also used that includes Gogny D1S in addition to a five-dimensional collective Hamiltonian (5DCH) [62,63]. The comparison of S_{2n} values from this work and those from the mass models is shown in Fig. 4(a).

Nuclear mass models for these masses are generally optimized with known masses and heavily rely on atomic mass databases. Most of the models compared in this work follow the trend of experimental data; however, only a few are able to reproduce the area of deformation or shape transition, i.e., the dip at $N = 59$.

In the region of $N > 61$, the differences between S_{2n} values from this work and different mass models are plotted in Fig. 4(b). As is evident from this figure, the DZ, FRDM12, and HFB24 models are in close agreement to AME2016 measured and extrapolated values, with FRDM12 having the largest deviation. These three models tend toward the extrapolated values of AME2016 and thus overpredict two-neutron separation energies for $N = 65$–67.

The beyond-mean-field calculation in D1S-5DCH agrees well with the experimental trend till $N = 58$ and then follows a continuous drop in binding energies throughout the $N = 58$–70 region. It fails to reproduce the shape transition at $N = 60$ and underpredicts the separation energies beyond $N = 58$. The calculations with Gogny interaction (D1S) follow the trend of S_{2n} energies throughout but underpredict for $N \geqslant 60$, with a larger offset than D1S-5DCH.

UNEDF0 gives the closest description of S_{2n} values in both Rb and Sr isotopes in this mass region. Rb isotopes follow the pattern well till $N = 66$ whereas Sr isotopes start diverting from UNEDF0 after $N = 66$, where UNEDF0 is also inclined toward extrapolated values and thus overpredicts S_{2n} energies. This model also predicted a smoother trend at $N = 66$ (mid-shell) nuclei against AME2016 extrapolations, and the new mass values confirm the trend. UNEDF1 follows the trend for both Rb and Sr isotopes, but there is an offset between UNEDF1 values and the experimental data. In Sr isotopes, experimental data tend to go closer toward UNEDF1 values at $N = 66$ and above.

S_{2n} data in this work indicate that neutrons are less bound for nearby $_{37}$Rb and $_{38}$Sr isotopes than expected from mass models and thus give a strong impetus to update the mass models.

In order to further investigate any structure changes, another important metric was considered, i.e., the neutron pairing gap D_n [64], which can be quantified as the difference between neutron separation energies of successive isotopes, given by $D_n(N) = (-1)^{N+1}[S_n(Z, N+1) - S_n(Z, N)]$. D_n is a sensitive tool to measure the changes in nuclear structure [65], and is directly related to the empirical neutron

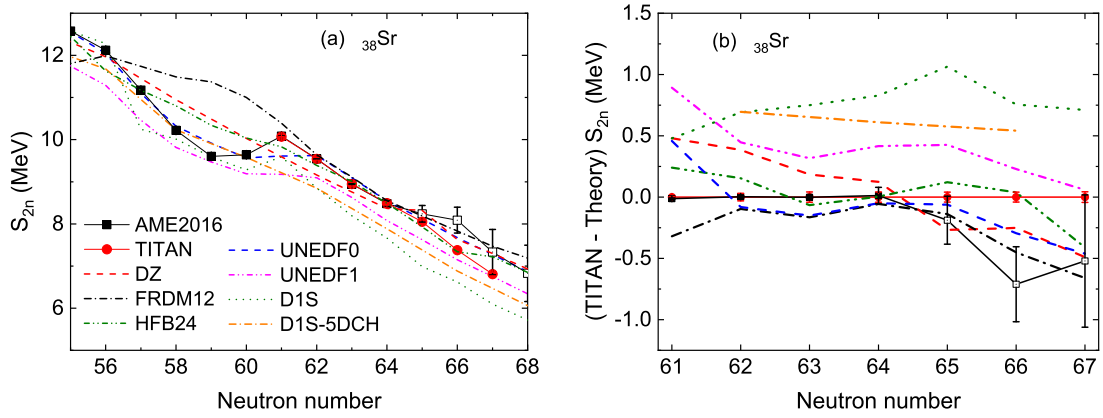

FIG. 4. (a) S_{2n} values for isotopes of $_{38}$Sr compared with values from different mass models, and (b) the differences between S_{2n} values from this work and different mass models. Circles and squares represent experimental and AME2016 values, respectively, with open squares being extrapolated values.

pairing gap $\Delta^3(N) = D_n(N)/2$ [66], also known as the odd-even staggering parameter. D_n values for isotopes of Rb and Sr from this work and AME2016 are shown in Fig. 5(a). The main features in this figure are (i) the sharp rise in D_n value at $N = 50$, indicating a shell closure, (ii) the change in staggering pattern at $N = 59$, indicating shape change or onset of deformation, and (iii) a consistent odd-even staggering after $N = 61$, indicating stability against shape changes.

There is no unusual change in D_n pattern in the vicinity of $N = 66$ for both Rb and Sr cases, indicating no further shape change or shell gap or onset of deformation. Our new values gives evidence of reduced neutron pairing in the mass surface near $N = 66$ for the Rb isotopic chains.

We also compared the behavior of D_n values from different mass models for Sr isotopes, as shown in Fig. 5(b). We selected mass models, namely, Duflo-Zuker [13], FRDM2012 [14], HFB24 [15], and UNEDF0 [58] that had closer agreement with experimental S_{2n} values from this work. All of these models show a consistent pattern in this mass region, whereas, except for UNEDF0, most of them over-predict D_n. UNEDF0 is the closest match till $N = 58$ in the measured mass territory, after which it overpredicts relative to the extrapolated values in AME2016 at $N = 65$.

B. Astrophysical discussion

The neutron separation energy, S_n, is a sensitive input for r-process calculations [12]. It is calculated from atomic mass using $S_n(N, Z) = -M(N, Z) + M(N - 1, Z) + m_n$, where m_n is the mass of the neutron. The neutron separation energies are directly used in the calculation of neutron capture rates and photodissociation rates. The latter's exponential dependence highlights the impact of masses on r-process calculations [1], as discussed in the following paragraphs.

To estimate the effect of the new masses on astrophysical r-process abundances, we calculated fractional abundances using the waiting-point approximation [2] for the isotopes of interest. At the equilibrium condition, the rate of neutron capture is equal to the rate of photo-disintegration, $(n, \gamma) = (\gamma, n)$. In this condition, the abundance distribution along the

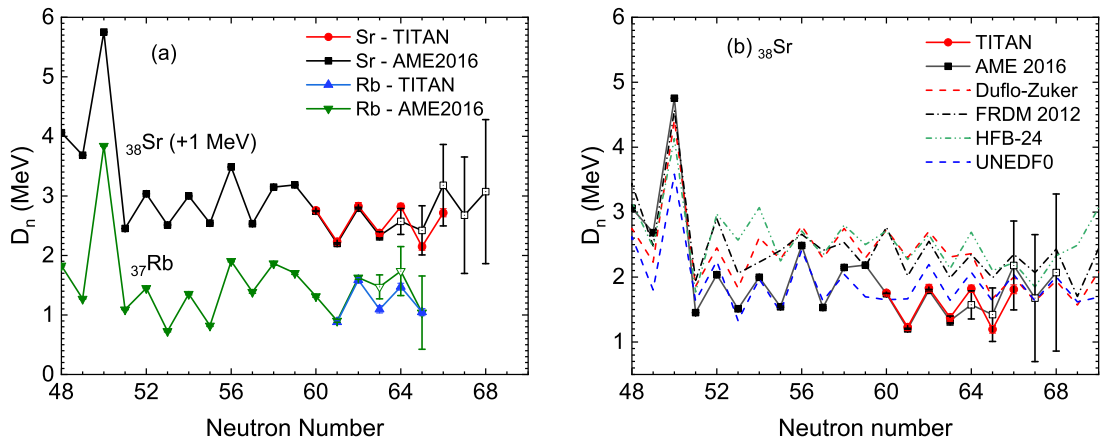

FIG. 5. (a) Two-neutron pairing gap D_n calculated from this work and AME2016 for Sr (shifted by 1 MeV for clarity) and Rb isotopes. Extrapolated values from AME2016 are denoted by open squares and triangles. Shell closure at $N = 50$ is clearly visible. (b) D_n for $_{38}$Sr isotopes compared with D_n values from different mass models.

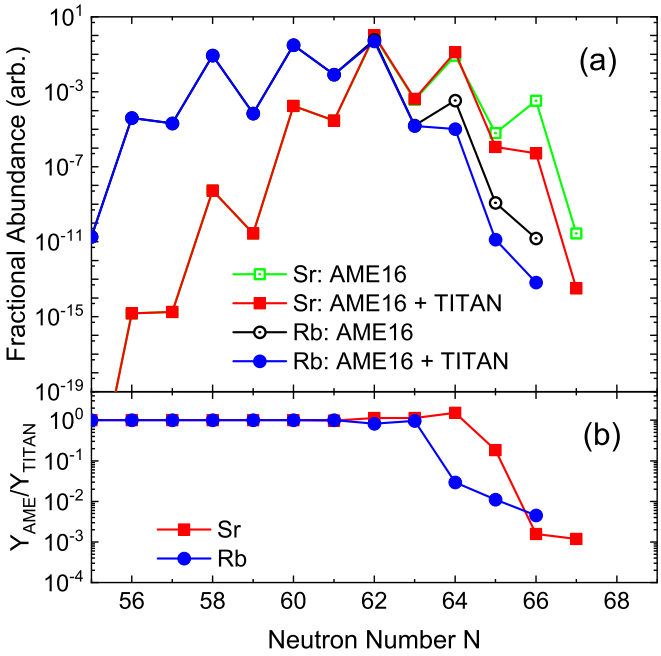

FIG. 6. (a) Fractional *r*-process abundance for Rb and Sr isotopes relative to most abundant isotopes using waiting point approximation. Open circles are values taken from AME2016. Filled circles denote a combination of values calculated from AME2016 values and new TITAN mass values from this work. (b) The ratio of fractional abundances ($Y_{\mathrm{AME2016}}/Y_{\mathrm{TITAN}}$) corresponding to values plotted in panel (a).

isotopic chain is entirely determined by the chemical potentials [10], and the abundance yields of neighboring nuclei can be calculated using the Saha equation given by

$$\frac{Y_1}{Y_2} = n_n \frac{G_1}{2G_2}\left(\frac{A+1}{A}\frac{2\pi\hbar^2}{m_u kT}\right)^{3/2} e^{S_n/kT}, \qquad (2)$$

here Y_i are the yields of the neighboring nuclei in the isotopic chain, G_i are the astrophysical partition functions, k is the Boltzmann constant, T is the temperature in K, m_u is the atomic mass unit, and A is the mass number. The precise mass values are input in this equation as neutron separation energy (S_n).

The partition functions G_i were obtained from the work of Rauscher *et al.* [67]. The data in this reference were tabulated for larger steps, and thus they were spline interpolated for calculations. The temperature was varied between 1 and 2 GK and neutron densities were in the range of 10^{20}–10^{25} cm^{-3} [2]. The calculations were compared for S_n calculated from this work and S_n from AME2016. Figure 6(a) displays the calculations with $n_n = 10^{20}$ cm^{-3} and $T = 1.2$ GK, at which the biggest difference in abundance pattern was observed.

In order to calculate fractional yields for a complete isotopic chain, the new TITAN mass values were replaced with AME2016 extrapolations in the AME2016 values, resulting in (AME2016+TITAN) values. The ratio of yields from (AME2016+TITAN) values to the AME2016 values is shown in the bottom part of Fig. 6. The lower yield due to new mass measurement may impact the small *r*-process peak in the $A = 100$ mass region, and help in the understanding of the *r* process. Moreover, the increasing deviation of mass values from AME's extrapolated values suggests the need for mass measurements of more neutron-rich nuclei in this mass region.

As stated earlier, *r*-process network calculations rely on nuclear mass models in the unknown mass territory. With an increase in neutron number, most of the mass model predictions deviate to large values and become less reliable. The sensitivity of masses on *r*-process nucleosynthesis has been reviewed in Ref. [11], and 500 keV has been ascertained as an optimum limit for rms error in mass models. As discussed above, the new masses from this work deviate by more than 500 keV/c^2 from AME2016 extrapolations and the mass models frequently used in *r*-process calculations. As most mass models overpredict the neutron separation energies of the Rb and Sr isotopes under investigation, a detailed network calculation is required for finding the impact of these masses on *r*-process nucleosynthesis, as suggested by our simple estimates from the Saha equation.

V. SUMMARY

We measured the masses of the isotopic chains of Rb and Sr using multiple-reflection time-of-flight mass spectroscopy: Rb in the range of $A = 99$–103 and Sr in the range of $A = 99$–105. Of these, ^{103}Rb and $^{103-105}$Sr have been measured for the first time. These measurements reduced the uncertainties for new masses to less than 45 keV/c^2. The deviation from AME2016 values with our values for ^{103}Rb is nearly 400 keV/c^2 and for $^{103-105}$Sr is 200–700 keV/c^2. We also confirm the deviation of mass value for ^{102}Rb with respect to AME2016, as reported by ISOLTRAP [30].

We compared the newly measured values from this work with those from existing literature and theoretical models through the nuclear mass surface and its derivatives, namely, the neutron separation energy, the neutron pairing gap, the two-neutron separation energy, and the two-neutron shell gap. For the measurements in this work, we obtained lower pairing gaps and lower neutron separation energies, suggesting loosely bound nuclei compared to values based on commonly used mass models. This also indicates that neutron rich isotopes of $Z = 37, 38$ will reach the neutron drip line earlier than expected. Our findings also refute the presence of a shell gap or the onset of deformation near mid-shell $N = 66$ in $_{37}$Rb and $_{38}$Sr isotopes. The new mass values have a deviation of more than 0.5 MeV from AME2016 extrapolations and nuclear mass models. These new values also affect the calculated fractional *r*-process abundance pattern as seen in the waiting-point approximation calculation.

ACKNOWLEDGMENTS

The authors acknowledge technical support from the staff at the TRILIS group, the ISAC beam delivery group, and M. Good for their contributions in realizing this experiment. The authors also thank V. Manea and D. Lunney for

fruitful discussions. This work has been supported by the Natural Sciences and Engineering Research Council of Canada (NSERC) and via TRIUMF the National Research Council (NRC) of Canada. E.D. acknowledges financial support from the U.K.-Canada foundation. M.P.R. acknowledges support from German institutions DFG (Grants No. FR 601/3-1 and No. SFB 1245 and through PRISMA Cluster of Excellence), BMBF (Grants No. 05P15RGFN1 and No. 05P12RGFN8), the Helmholtz Association through NAVI (Grant No. VH-VI-417), HMWK through the LOEWE Center HICforFAIR, by the Justus Liebig Universität Gießen from Germany and GSI under the JLU-GSI strategic Helmholtz partnership agreement. E.L. acknowledges financial support from Brazil's CNPq (Grant No. 249121/2013-1). M.B. acknowledge support by the National Science Foundation (NSF) under Grants No. PHY-1713857 and No. PHY-2011890.

[1] E. M. Burbidge, G. R. Burbidge, W. A. Fowler, and F. Hoyle, Synthesis of the elements in stars, Rev. Mod. Phys. **29**, 547 (1957).

[2] J. J. Cowan, F.-K. Thielemann, and J. W. Truran, The r-process and nucleochronology, Phys. Rep. **208**, 267 (1991).

[3] National Research Council 2003, *Connecting Quarks with the Cosmos: Eleven Science Questions for the New Century* (The National Academies, Washington, DC, 2003).

[4] M. Arnould, S. Goriely, and K. Takahashi, The r-process of stellar nucleosynthesis: Astrophysics and nuclear physics achievements and mysteries, Phys. Rep. **450**, 97 (2007).

[5] J. J. Cowan, C. Sneden, J. E. Lawler, A. Aprahamian, M. Wiescher, K. Langanke, G. Martínez-Pinedo, and F.-K. Thielemann, Making the heaviest elements in the universe: A review of the rapid neutron capture process, Rev. Mod. Phys. **93**, 015002 (2021).

[6] D. A. Coulter, R. J. Foley, C. D. Kilpatrick, M. R. Drout, A. L. Piro, B. J. Shappee, M. R. Siebert, J. D. Simon, N. Ulloa, D. Kasen, B. F. Madore, A. Murguia-Berthier, Y.-C. Pan, J. X. Prochaska, E. Ramirez-Ruiz, A. Rest, and C. Rojas-Bravo, Swope Supernova Survey 2017a (SSS17a), the optical counterpart to a gravitational wave source, Science **358**, 1556 (2017).

[7] B. P. Abbott, R. Abbott, T. D. Abbott, F. Acernese, K. Ackley, C. Adams, T. Adams, P. Addesso, R. X. Adhikari, V. B. Adya, C. Affeldt, M. Afrough *et al.*, Multi-messenger observations of a binary neutron star merger, Astrophys. J. **848**, L12 (2017).

[8] B. P. Abbott, R. Abbott, T. D. Abbott, F. Acernese, K. Ackley, C. Adams, T. Adams, P. Addesso, R. X. Adhikari, V. B. Adya, C. Affeldt, M. Afrough, B. Agarwal, M. Agathos, K. Agatsuma, N. Aggarwal, O. D. Aguiar, L. Aiello, A. Ain, P. Ajith *et al.*, Gravitational waves and gamma-rays from a binary neutron star merger: GW170817 and GRB 170817a, Astrophys. J. **848**, L13 (2017).

[9] D. Watson, C. J. Hansen, J. Selsing, A. Koch, D. B. Malesani, A. C. Andersen, J. P. U. Fynbo, A. Arcones, A. Bandswein, S. Covino, A. Grado, K. E. Heintz, L. Hunt, C. Kouveliotou, G. Leloudas, A. J. Levan, P. Mazzali, and E. Pian, Identification of strontium in the merger of two neutron stars, Nature (London) **574**, 497 (2019).

[10] H. Schatz, Nuclear masses in astrophysics, Int. J. Mass Spectrom. **349-350**, 181 (2013), 100 years of Mass Spectrometry.

[11] M. R. Mumpower, R. Surman, G. McLaughlin, and A. Aprahamian, The impact of individual nuclear properties on r-process nucleosynthesis, Prog. Part. Nucl. Phys. **86**, 86 (2016).

[12] M. R. Mumpower, R. Surman, D.-L. Fang, M. Beard, P. Möller, T. Kawano, and A. Aprahamian, Impact of individual nuclear masses on *r*-process abundances, Phys. Rev. C **92**, 035807 (2015).

[13] J. Duflo and A. P. Zuker, Microscopic mass formulas, Phys. Rev. C **52**, R23 (1995).

[14] P. Möller, W. D. Myers, H. Sagawa, and S. Yoshida, New Finite-Range Droplet Mass Model and Equation-of-State Parameters, Phys. Rev. Lett. **108**, 052501 (2012).

[15] S. Goriely, N. Chamel, and J. M. Pearson, Further explorations of Skyrme-Hartree-Fock-Bogoliubov mass formulas. XIII. The 2012 atomic mass evaluation and the symmetry coefficient, Phys. Rev. C **88**, 024308 (2013).

[16] W. Huang, G. Audi, M. Wang, F. G. Kondev, S. Naimi, and X. Xu, The AME2016 atomic mass evaluation (I). evaluation of input data and adjustment procedures, Chin. Phys. C **41**, 030002 (2017).

[17] I. Angeli and K. Marinova, Table of experimental nuclear ground state charge radii: An update, At. Data Nucl. Data Tables **99**, 69 (2013).

[18] F. Buchinger, E. B. Ramsay, E. Arnold, W. Neu, R. Neugart, K. Wendt, R. E. Silverans, P. Lievens, L. Vermeeren, D. Berdichevsky, R. Fleming, D. W. L. Sprung, and G. Ulm, Systematics of nuclear ground state properties in $^{78-100}$Sr by LASER spectroscopy, Phys. Rev. C **41**, 2883 (1990).

[19] P. Lievens, R. Silverans, L. Vermeeren, W. Borchers, W. Neu, R. Neugart, K. Wendt, F. Buchinger, and E. Arnold, Nuclear ground state properties of ^{99}Sr by collinear laser spectroscopy with non-optical detection, Phys. Lett. B **256**, 141 (1991).

[20] B. Cheal, M. Gardner, M. Avgoulea, J. Billowes, M. Bissell, P. Campbell, T. Eronen, K. Flanagan, D. Forest, J. Huikari, A. Jokinen, B. Marsh, I. Moore, A. Nieminen, H. Penttilä, S. Rinta-Antila, B. Tordoff, G. Tungate, and J. Äystö, The shape transition in the neutron-rich yttrium isotopes and isomers, Phys. Lett. B **645**, 133 (2007).

[21] P. Campbell, H. L. Thayer, J. Billowes, P. Dendooven, K. T. Flanagan, D. H. Forest, J. A. R. Griffith, J. Huikari, A. Jokinen, R. Moore, A. Nieminen, G. Tungate, S. Zemlyanoi, and J. Äystö, Laser Spectroscopy of Cooled Zirconium Fission Fragments, Phys. Rev. Lett. **89**, 082501 (2002).

[22] C. Thibault, F. Touchard, S. Büttgenbach, R. Klapisch, M. de Saint Simon, H. T. Duong, P. Jacquinot, P. Juncar, S. Liberman, P. Pillet, J. Pinard, J. L. Vialle, A. Pesnelle, and G. Huber, Hyperfine structure and isotope shift of the D_2 line of $^{76-98}$Rb and some of their isomers, Phys. Rev. C **23**, 2720 (1981).

[23] M. Keim, E. Arnold, W. Borchers, U. Georg, A. Klein, R. Neugart, L. Vermeeren, R. Silverans, and P. Lievens, Laser-spectroscopy measurements of $^{72-96}$Kr spins, moments and charge radii, Nucl. Phys. A **586**, 219 (1995).

[24] R. Rodríguez-Guzmán, P. Sarriguren, L. Robledo, and S. Perez-Martin, Charge radii and structural evolution in Sr, Zr, and Mo isotopes, Phys. Lett. B **691**, 202 (2010).

[25] J. Xiang, Z. Li, Z. Li, J. Yao, and J. Meng, Covariant description of shape evolution and shape coexistence in neutron-rich nuclei at N≈60, Nucl. Phys. A **873**, 1 (2012).

[26] U. Hager, T. Eronen, J. Hakala, A. Jokinen, V. S. Kolhinen, S. Kopecky, I. Moore, A. Nieminen, M. Oinonen, S. Rinta-Antila,

J. Szerypo, and J. Äystö, First Precision Mass Measurements of Refractory Fission Fragments, Phys. Rev. Lett. **96**, 042504 (2006).

[27] S. Naimi, G. Audi, D. Beck, K. Blaum, C. Böhm, C. Borgmann, M. Breitenfeldt, S. George, F. Herfurth, A. Herlert, M. Kowalska, S. Kreim, D. Lunney, D. Neidherr, M. Rosenbusch, S. Schwarz, L. Schweikhard, and K. Zuber, Critical-Point Boundary for the Nuclear Quantum Phase Transition Near $A = 100$ from Mass Measurements of ^{96,97}Kr, Phys. Rev. Lett. **105**, 032502 (2010).

[28] V. V. Simon, T. Brunner, U. Chowdhury, B. Eberhardt, S. Ettenauer, A. T. Gallant, E. Mané, M. C. Simon, P. Delheij, M. R. Pearson, G. Audi, G. Gwinner, D. Lunney, H. Schatz, and J. Dilling, Penning-trap mass spectrometry of highly charged, neutron-rich Rb and Sr isotopes in the vicinity of $A \approx 100$, Phys. Rev. C **85**, 064308 (2012).

[29] V. Manea, D. Atanasov, D. Beck, K. Blaum, C. Borgmann, R. B. Cakirli, T. Eronen, S. George, F. Herfurth, A. Herlert, M. Kowalska, S. Kreim, Y. A. Litvinov, D. Lunney, D. Neidherr, M. Rosenbusch, L. Schweikhard, F. Wienholtz, R. N. Wolf, and K. Zuber, Collective degrees of freedom of neutron-rich $A \approx 100$ nuclei and the first mass measurement of the short-lived nuclide ^{100}Rb, Phys. Rev. C **88**, 054322 (2013).

[30] A. de Roubin, D. Atanasov, K. Blaum, S. George, F. Herfurth, D. Kisler, M. Kowalska, S. Kreim, D. Lunney, V. Manea, E. Minaya Ramirez, M. Mougeot, D. Neidherr, M. Rosenbusch, L. Schweikhard, A. Welker, F. Wienholtz, R. N. Wolf, and K. Zuber, Nuclear deformation in the $A \approx 100$ region: Comparison between new masses and mean-field predictions, Phys. Rev. C **96**, 014310 (2017).

[31] R. Klawitter, A. Bader, M. Brodeur, U. Chowdhury, A. Chaudhuri, J. Fallis, A. T. Gallant, A. Grossheim, A. A. Kwiatkowski, D. Lascar, K. G. Leach, A. Lennarz, T. D. Macdonald, J. Pearkes, S. Seeraji, M. C. Simon, V. V. Simon, B. E. Schultz, and J. Dilling, Mass measurements of neutron-rich Rb and Sr isotopes, Phys. Rev. C **93**, 045807 (2016).

[32] D. Lunney, J. M. Pearson, and C. Thibault, Recent trends in the determination of nuclear masses, Rev. Mod. Phys. **75**, 1021 (2003).

[33] K. Blaum, J. Dilling, and W. Nörtershäuser, Precision atomic physics techniques for nuclear physics with radioactive beams, Phys. Scr. **T152**, 014017 (2013).

[34] J. Dilling, K. Blaum, M. Brodeur, and S. Eliseev, Penning-trap mass measurements in atomic and nuclear physics, Annu. Rev. Nucl. Part. Sci. **68**, 45 (2018).

[35] J. Dilling, R. Baartman, P. Bricault, M. Brodeur, L. Blomeley, F. Buchinger, J. Crawford, J. R. C. López-Urrutia, P. Delheij, M. Froese, G. Gwinner, Z. Ke, J. Lee, R. Moore, V. Ryjkov, G. Sikler, M. Smith, J. Ullrich, and J. Vaz, Mass measurements on highly charged radioactive ions, a new approach to high precision with TITAN, Int. J. Mass Spectrom. **251**, 198 (2006).

[36] A. A. Kwiatkowski, C. Andreoiu, J. C. Bale, T. Brunner, A. Chaudhuri, U. Chowdhury, P. Delheij, S. Ettenauer, D. Frekers, A. T. Gallant, A. Grossheim, G. Gwinner, F. Jang, A. Lennarz, T. Ma, E. Mané, M. R. Pearson, B. E. Schultz, M. C. Simon, V. V. Simon *et al.*, TITAN: An ion trap facility for on-line mass measurement experiments, Hyperfine Interact. **225**, 143 (2014).

[37] C. Jesch, T. Dickel, W. R. Plaß, D. Short, S. Ayet San Andres, J. Dilling, H. Geissel, F. Greiner, J. Lang, K. G. Leach, W. Lippert, C. Scheidenberger, and M. I. Yavor, The MR-TOF-MS isobar separator for the TITAN facility at TRIUMF, Hyperfine Interact. **235**, 97 (2015).

[38] T. Dickel, S. A. San Andrés, S. Beck, J. Bergmann, J. Dilling, F. Greiner, C. Hornung, A. Jacobs, G. Kripko-Koncz, A. Kwiatkowski, E. Leistenschneider, A. Pikthtelev, W. R. Plaß, M. P. Reiter, C. Scheidenberger, C. Will, and the TITAN Collaboration, Isobar separation in a multiple-reflection time-of-flight mass spectrometer by mass-selective re-trapping, Hyperfine Interact. **240**, 62 (2019).

[39] J. Dilling, R. Krücken, and L. Merminga, *ISAC and ARIEL: The TRIUMF Radioactive Beam Facilities and the Scientific Program* (Springer, Dordrecht, 2014).

[40] P. Kunz, P. Bricault, M. Dombsky, N. Erdmann, V. Hanemaayer, J. Wong, and K. Lützenkirchen, Composite uranium carbide targets at TRIUMF: Development and characterization with SEM, XRD, XRF and L-edge densitometry, J. Nucl. Mater. **440**, 110 (2013).

[41] J. Lassen, P. Bricault, M. Dombsky, J. P. Lavoie, M. Gillner, T. Gottwald, F. Hellbusch, A. Teigelhöfer, A. Voss, and K. D. A. Wendt, Laser ion source operation at the TRIUMF radioactive ion beam facility, in *4th International Conference on Laser Probing–LAP 2008, 6–10 October 2008, Nagoya, Japan*, edited by T. Iguchi and K. Watanabe, AIP Conf. Proc. No. 1104 (AIP, New York, 2009), p. 9.

[42] T. Brunner, M. Smith, M. Brodeur, S. Ettenauer, A. Gallant, V. Simon, A. Chaudhuri, A. Lapierre, E. Mané, R. Ringle, M. Simon, J. Vaz, P. Delheij, M. Good, M. Pearson, and J. Dilling, TITAN's digital RFQ ion beam cooler and buncher, operation and performance, Nucl. Instrum. Methods Phys. Res., Sect. A **676**, 32 (2012).

[43] M. Smith, L. Blomeley, P. Delheij, and J. Dilling, First tests of the TITAN digital RFQ beam cooler and buncher, Hyperfine Interact. **173**, 171 (2006).

[44] W. R. Plass, T. Dickel, S. A. S. Andres, J. Ebert, F. Greiner, C. Hornung, C. Jesch, J. L. andW. Lippert, T.Majoros, D. Short, H. Geissel, E. Haettner, M. P.Reiter, A.-K.Rink, C. Scheidenberger, and M. I. Yavor, High-performance multiple-reflection time-of-flight mass spectrometers for research with exotic nuclei and for analytical mass spectrometry, Phys. Scr. **T166**, 014069 (2015).

[45] M. I. Yavor, W. R. Plaß, T. Dickel, H. Geissel, and C. Scheidenberger, Ion-optical design of a high-performance multiple-reflection time-of-flight mass spectrometer and isobar separator, Int. J. Mass Spectrom. **381-382**, 1 (2015).

[46] H. Wollnik and M. Przewloka, Time-of-flight mass spectrometers with multiply reflected ion trajectories, Int. J. Mass Spectrom. Ion Processes **96**, 267 (1990).

[47] T. Dickel, M. I. Yavor, J. Lang, W. R. Plaß, W. Lippert, H. Geissel, and C. Scheidenberger, Dynamical time focus shift in multiple-reflection time-of-flight mass spectrometers, Int. J. Mass Spectrom. **412**, 1 (2017).

[48] T. Dickel, W. R. Plaß, W. Lippert, J. Lang, M. I. Yavor, H. Geissel, and C. Scheidenberger, Isobar separation in a multiple-reflection time-of-flight mass spectrometer by mass-selective re-trapping, J. Am. Soc. Mass Spectrom. **28**, 1079 (2017).

[49] S. Beck *et al.* (unpublished).

[50] S. Ayet San Andrés, C. Hornung, J. Ebert, W. R. Plaß, T. Dickel, H. Geissel, C. Scheidenberger, J. Bergmann, F. Greiner, E. Haettner, C. Jesch, W. Lippert, I. Mardor, I. Miskun, Z. Patyk, S. Pietri, A. Pihktelev, S. Purushothaman, M. P. Reiter, A.-K. Rink *et al.*, High-resolution, accurate multiple-reflection

time-of-flight mass spectrometry for short-lived, exotic nuclei of a few events in their ground and low-lying isomeric states, Phys. Rev. C **99**, 064313 (2019).

[51] E. Leistenschneider, M. P. Reiter, S. Ayet San Andrés, B. Kootte, J. D. Holt, P. Navrátil, C. Babcock, C. Barbieri, B. R. Barquest, J. Bergmann, J. Bollig, T. Brunner, E. Dunling, A. Finlay, H. Geissel, L. Graham, F. Greiner, H. Hergert, C. Hornung, C. Jesch *et al.*, Dawning of the $N = 32$ Shell Closure Seen through Precision Mass Measurements of Neutron-Rich Titanium Isotopes, Phys. Rev. Lett. **120**, 062503 (2018).

[52] ENSDF, https://www.nndc.bnl.gov/ensdf/, accessed 2020-04-03.

[53] M. Wang, G. Audi, F. G. Kondev, W. Huang, S. Naimi, and X. Xu, The AME2016 atomic mass evaluation (II). Tables, graphs and references, Chin. Phys. C **41**, 030003 (2017).

[54] R. Barden, R. Kirchner, O. Klepper, A. Plochocki, G. E. Rathke, E. Roeckl, K. Rykaczewski, D. Schardt, and J. Zylicz, The Gamow-Teller beta decay of neutron-deficient even isotopes of tin, Z. Phys. A: At. Nucl. **329**, 319 (1988).

[55] F. Browne, A. Bruce, T. Sumikama, I. Nishizuka, S. Nishimura, P. Doornenbal, G. Lorusso, P.-A. Söderström, H. Watanabe, R. Daido, Z. Patel, S. Rice, L. Sinclair, J. Wu, Z. Xu, A. Yagi, H. Baba, N. Chiga, R. Carroll, F. Didierjean *et al.*, Lifetime measurements of the first 2^+ states in ^{104,106}Zr: Evolution of ground-state deformations, Phys. Lett. B **750**, 448 (2015).

[56] M. Albers, K. Nomura, N. Warr, A. Blazhev, J. Jolie, D. Mücher, B. Bastin, C. Bauer, C. Bernards, L. Bettermann, V. Bildstein, J. Butterworth, M. Cappellazzo, J. Cederkäll, D. Cline, I. Darby, S. D. Gupta, J. Daugas, T. Davinson, H. D. Witte *et al.*, Shape dynamics in neutron-rich Kr isotopes: Coulomb excitation of ^{92}Kr, ^{94}Kr and ^{96}Kr, Nucl. Phys. A **899**, 1 (2013).

[57] M. Bender, P.-H. Heenen, and P.-G. Reinhard, Self-consistent mean-field models for nuclear structure, Rev. Mod. Phys. **75**, 121 (2003).

[58] M. Kortelainen, T. Lesinski, J. Moré, W. Nazarewicz, J. Sarich, N. Schunck, M. V. Stoitsov, and S. Wild, Nuclear energy density optimization, Phys. Rev. C **82**, 024313 (2010).

[59] M. Kortelainen, J. McDonnell, W. Nazarewicz, P.-G. Reinhard, J. Sarich, N. Schunck, M. V. Stoitsov, and S. M. Wild, Nuclear energy density optimization: Large deformations, Phys. Rev. C **85**, 024304 (2012).

[60] J. Dechargé and D. Gogny, Hartree-Fock-Bogolyubov calculations with the $d1$ effective interaction on spherical nuclei, Phys. Rev. C **21**, 1568 (1980).

[61] J. Berger, M. Girod, and D. Gogny, Time-dependent quantum collective dynamics applied to nuclear fission, Comput. Phys. Commun. **63**, 365 (1991).

[62] G. F. Bertsch, M. Girod, S. Hilaire, J.-P. Delaroche, H. Goutte, and S. Péru, Systematics of the First 2^+ Excitation with the Gogny Interaction, Phys. Rev. Lett. **99**, 032502 (2007).

[63] J. P. Delaroche, M. Girod, J. Libert, H. Goutte, S. Hilaire, S. Péru, N. Pillet, and G. F. Bertsch, Structure of even-even nuclei using a mapped collective hamiltonian and the D1S Gogny interaction, Phys. Rev. C **81**, 014303 (2010).

[64] B. A. Brown, Nuclear Pairing Gap: How Low Can It Go? Phys. Rev. Lett. **111**, 162502 (2013).

[65] J. Hakala, J. Dobaczewski, D. Gorelov, T. Eronen, A. Jokinen, A. Kankainen, V. S. Kolhinen, M. Kortelainen, I. D. Moore, H. Penttilä, S. Rinta-Antila, J. Rissanen, A. Saastamoinen, V. Sonnenschein, and J. Äystö, Precision Mass Measurements Beyond ^{132}Sn: Anomalous Behavior of Odd-Even Staggering of Binding Energies, Phys. Rev. Lett. **109**, 032501 (2012).

[66] W. Satuła, J. Dobaczewski, and W. Nazarewicz, Odd-Even Staggering of Nuclear Masses: Pairing or Shape Effect? Phys. Rev. Lett. **81**, 3599 (1998).

[67] T. Rauscher and F.-K. Thielemann, Astrophysical reaction rates from statistical model calculations, At. Data Nucl. Data Tables **75**, 1 (2000).